Title

Silicon incorporation in polymethine dyes

Permalink

https://escholarship.org/uc/item/5b4155nz

Journal

Chemical Communications, 56(45)

ISSN

1359-7345

Authors

Pengshung, Monica
Neal, Patrick
Atallah, Timothy L
et al.

Publication Date

2020-06-07

DOI

10.1039/c9cc09671j

Peer reviewed

Silicon incorporation in polymethine dyes

Monica Pengshung[a], **Patrick Neal**[b], **Timothy L. Atallah**[a], **Junho Kwon**[a], **Justin R. Caram**[a,*], **Steven A. Lopez**[b,*], **Ellen M. Sletten**[a,*]

[a.]Department of Chemistry and Biochemistry, University of California, Los Angeles, CA 90095

[b.]Department of Chemistry and Chemical Biology, Northeastern University, 360 Huntington Avenue, Boston, Massachusetts 02115, United States

Abstract

Methods to red-shift fluorophores have garnered considerable interest due to the broad utility of low energy light. The incorporation of silicon into xanthene and coumarin scaffolds has resulted in an array of visible and near-infrared fluorophores. Here, we extend this approach to polymethine dyes, another popular fluorophore class, performing experimental and computational analyses. We found that when oxygen was replaced with $SiMe_2$, bathochromic shifts of up to 121 nm and fluorophores with emission above 900 nm were achieved.

Graphical Abstract
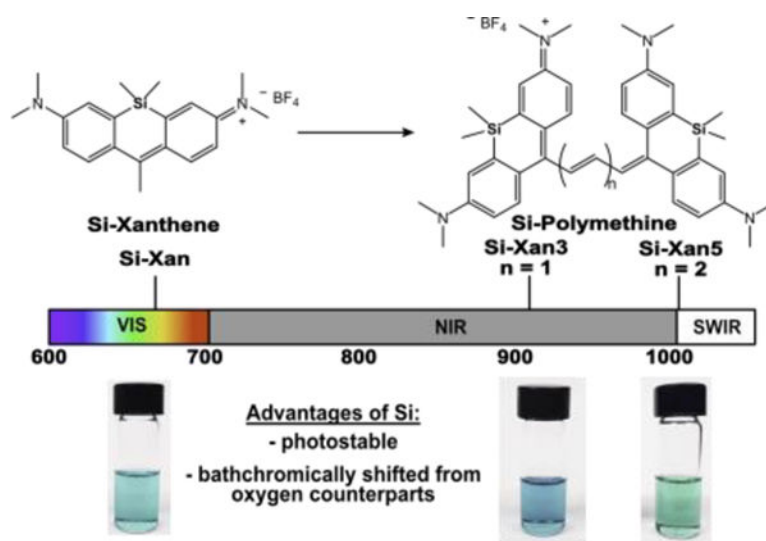
Conflicts of interest
There are no conflicts to declare.

Notes

Fluorescence is a vital research tool for analysing molecules in complex, dilute environments.[1] Key to the success of fluorescent analyses are fluorophores. Classic fluorophore scaffolds include polycyclic aromatic hydrocarbon, coumarin, fluorescein, rhodamine, and cyanine dyes.[1] Collectively, these fluorophores have enabled fundamental materials and biological studies; however, due to limitations of light penetration through heterogeneous materials, there has been interest in red-shifting fluorophores to the near-infrared (NIR, 700–1000 nm) region and beyond.[2,3]

In 2008, Xu and coworkers reported that the introduction of silicon into a xanthene chromophore in place of oxygen resulted in a bathochromic shift of 100 nm (Figure 1A).[4] The red-shift imparted by silicon has been attributed to a low-lying lowest unoccupied molecular orbital (LUMO).[5] Following this initial work, the use of silicon to red-shift fluorophores has been applied to oxazine, coumarin, fluorescein and rhodamine dyes (Figure 1B, C, D).[6–11] These silicon-containing fluorophores have been shown to be bright probes with advantageous photostability. We now extend silicon incorporation to another ubiquitous class of fluorophores, polymethine dyes, for the first time.

Polymethine dyes are known for their narrow absorption bands, high absorption coefficients, and readily tunable λ_{max} within the visible and near-infrared regions. The most common polymethines are cyanine dyes, which have nitrogen-containing heterocycles connected via a polymethine chain (Figure 1E). A widely utilized approach to significantly modulate the λ_{max} of cyanine dyes is to vary the length of the polymethine chain, which leads to a ~100 nm red-shift for each additional vinylene unit, though this often decreases stability.[12] An alternative strategy to afford large red-shifts is to replace the nitrogen with a different heteroatom which has yielded polymethine dyes containing O, S, Se, and Te but surprisingly not Si despite its popularity in other fluorophore scaffolds.[14] Herein, we demonstrate that the incorporation of silicon into heterocycles for polymethine dyes can impart red-shifts of similar magnitude to extension of the polymethine chain, while also enhancing photostability, resulting in fluorophores with emission above 900 nm (Figure 1F).

To prepare polymethine fluorophores, heterocycles that can readily react with electrophilic polyene linkers are necessary. We synthesized xanthone **1** according to literature procedures[15] and treated it with MeMgBr (Scheme 1A) to obtain **3**, an appropriate heterocycle for polymethine dye synthesis. Additionally, silicon xanthylium **3** proved to be a bright new fluorophore with $\lambda_{max,abs}$ = 646 nm and $\lambda_{max,ems}$ = 673 nm (Figure 2A, blue). Notably, this is 100 nm red-shifted from the oxygen congener **4**, which we synthesized as a control (Scheme 1A).

To synthesize the first generation of silicon polymethines, **3** was deprotonated with 2,6-lutidine and combined with diphenylformamidinine (**5**) in acetic anhydride (Scheme 1B) to afford **7** as a dark blue solid. Trimethine **7** displayed an absorption band that ranged from 550–950 nm with $\lambda_{max,abs}$ at 854 nm and $\lambda_{max,ems}$ at 913 nm (Figures 2A, S1A, red). We prepared pentamethine dye **10** through a similar procedure substituting diphenylformamidinine with malonaldehyde bis(phenylimine) HCl (**9**) to yield **10** (Scheme 1B). Pentamethine **10** had a similar absorption band to **7** extending from 550 nm to 1000 nm with a $\lambda_{max,abs}$ at 938 nm and $\lambda_{max,ems}$ at 1006 nm (Figures 2A, S1B, black).

Silicon polymethines **7** and **10** displayed a large absorption range (550–1000 nm) and contained two distinct peaks at 663 nm, and either 854 nm or 938 nm for **7** and **10**, respectively (Figure 2A). These spectra are uncharacteristic of traditional cyanine dyes, which generally have a narrow absorbance due to complete electron delocalization (Figure 3A).[16] Broad absorption spectra has been observed in long chain cyanine dyes (>7 carbon units) due to ground state desymmetrization in which electron delocalization within the polymethine is compromised such that asymmetric electronic configurations and dipolar character are observed (Figure 3B).[16,17] Shorter chain polymethine dyes containing xanthene heterocycles have also been reported to display ground state destabilization, resulting in bimodal absorbance spectra.[18]

As seen in Figure 2A, the absorbance spectra of pentamethine **10** in dichloromethane (DCM) displays a peak ratio of 1:1.5 for absorbance at 663 nm and 938 nm. The peak ratio is concentration independent (Figure S2), leading us to hypothesize the bimodal absorbance is due to the presence of asymmetric and symmetric states, respectively. We performed a solvatochromism study on **10** (Figure 3A), which revealed that the ratio of these peaks changed drastically with solvent polarity (Figure 3C). Polar solvents such as dimethyl sulfoxide and acetonitrile resulted in the 633 nm peak dominating by 2.5 fold. These results are consistent with previous findings that polar environments are able to stabilize the asymmetric state.[19] To more systematically study the effect of solvent polarity, we supplemented tetrahydrofuran (THF) containing **10** with more polar water or less polar chloroform (Figures 3E, 3F, respectively) which show opposite trends when increasing amounts of polar (water) or non-polar (chloroform) solvent are added. Mixtures of THF and phosphate buffered saline show similar dominance of the 633 nm peak (Figure S3). Trimethine **7** behaves comparably to **10** in solvatochromism studies (Figure S4). Interestingly, the $\lambda_{\text{max,abs}}$ of the asymmetric state of trimethine **7** is similar to pentamethine **10**, while their symmetric states differ by 84 nm. We attribute this to the asymmetric state having significant heterocycle character, with the heterocycle being a good chromophore itself.

To further explore the hypothesis of ground state desymmetrization, we employed quantum mechanical calculations. We first performed a conformational search to identify the global and local minima of **10**. These structures were then optimized with the hybrid density functional M06–2X[20] with the 6–31+G(d,p) basis set in gas phase and implicit solvent H_2O using Gaussian 16.[21] No gas phase geometries exhibited structural asymmetries nor did the lowest energy conformer in H_2O (**10-H_2O-A**), however two accessible solvated conformers **10-H_2O-B** and **10-H_2O-C** at 0.6 and 1.5 kcal mol^{-1} higher in free energy, respectively, were found to display asymmetry (Figure S5). Computationally, bond length alternation (BLA) and charge alternation (CA) are characteristic metrics for assessing ground state desymmetrization.[18] Analysis found that **10-H_2O-B** displayed BLA and CA (Figure S6A,B). However, the desymmetrization is small in magnitude, with 0.17e (elementary charge) asymmetrically transferred to one heterocycle (Figure 4A).

Therefore, we considered the role of dynamic structures resulting from accessible vibrational modes to simulate absorbance spectra (Figure S7). Vertical excitations, calculated with configuration interaction of singles with a correction to doubles method

[CIS(D)][22,23] with the cc-pvdz basis set and Resolution of the Identity (-RI) technique in ORCA 4.0.1[24,25] were computed on 50 Wigner sampled structures from the lowest energy *anti* and *syn* conformers of **10**.[‡] Structures with the most red-shifted λ_{max}, show complete electron delocalization of the highest occupied molecular orbital (HOMO) and LUMO (Figure 4B), whereas sampled geometries shifted to the 550–700 nm region show a desymmetrized HOMO and LUMO (Figure 4C). In the desymmetrized structures, the electron density is localized on the heterocycle, consistent with the experimentally observed peak at 663 nm. As such, the frontier molecular orbital calculations support the presence of an asymmetric state.

While the absorption of the silicon-containing polymethine dyes was broad and bimodal, the emission was well-defined with $\lambda_{max,ems} = 913$ nm for **7** and 1006 nm for **10** (Figure 2). The fluorescence quantum yields (Φ_F) were characterized to be 0.26% ± 0.02% and 0.19% ± 0.01% in DCM for **7** and **10**, respectively. Excited state lifetimes for **7** and **10** were 48 and 43 ps, consistent with their low Φ_F (Figure 2, Figure S8). Note that Φ_F for fluorophores above 900 nm are often quite low due to the small energy gap between the ground state and excited state.[26] The narrow emission band that does not mirror the absorption spectra is attributed to emission solely from the symmetrical state, which was confirmed with the excitation spectra for both **7** and **10** (Figure 3D, grey, S4).[27]

To showcase the direct benefit of silicon incorporation into the polymethine scaffold, we prepared oxygen congeners **8** and **11** (Scheme 1B, Figure S9). The silicon-containing polymethines showed significant bathochromic shifts compared to their oxygen analogues (Figures, 5A, 4B). The red-shift of λ_{max} between silicon fluorophores and oxygen is normally attributed to a lowered LUMO energy, caused by σ*–π* conjugation.[5] However, our calculations of **10** and **11** suggest that the LUMO of **11** is higher in energy than **10** because of a destabilizing out-of-phase interaction between the oxygen lone pair and the π orbitals in **11**, resulting in absorption at a higher energy for **11** than **10** (Figure S10).

We found that the degree of bathochromic shift between the O and Si containing fluorophores decreased as the polymethine linker increased. The absorbance difference at λ_{max} for the trimethines was 79 nm (1194 cm^{-1}) while the pentamethines was only 42 nm (500 cm^{-1}) (Figure 5A). Figure 5B shows that the degree of red-shifted emission spectra is larger for the trimethines than the pentamethines ($\lambda_{max} = 121$ and 71 nm, respectively). The smaller shifts in absorbance are likely due to contributions from the asymmetric state. We conclude that that the incorporation of silicon into polymethine fluorophores in place of oxygen results in bathochromic shifts of the symmetric state by 70–100 nm, on par with extension of the polymethine chain. These values are also consistent with previous reports of incorporation of silicon into other fluorophore scaffolds.[9,10]

Finally, another advantage commonly cited for the use of silicon fluorophores is an increased photostability.[6,9] We evaluated the photostability of the silicon fluorophores

---

[‡]We classified structures with polymethine substituents pointed away from each as *anti*, while structures with polymethine substituents pointed towards each other as *syn*.

compared to their oxygen analogues, focusing on the pair that has the most similar absorption: trimethine **7** and pentamethine **11** (Figure 5C).

Photobleaching of **7** and **11** was performed by continuous irradiation with a 730 nm LED (146 mW/cm^2). We found that **11** began photobleaching rapidly within the first hour while **7** was unchanged over three hours (Figure 5D). Upon calculation of the photobleaching rate constants, we found silicon-containing polymethine **7** to be six-fold more stable than **11** (Figure S11). Photobleaching of silicon pentamethine **10** under the same conditions showed a similar decrease as **7** (Figure S11), suggestive that silicon incorporation plays an important role in increasing the photostability. In comparison to other commercial fluorophores, **7** was more stable than 1,1′,3,3,3′,3′-Hexamethylindotricarbocyanine iodide (HITCI) but less stable than Rhodamine B (Figure S11).

Intrigued by these results, we further explored the pathways of degradation for these dyes. Photobleaching of cyanines are generally caused by $^1O_2$ mediated photolysis of the polymethine chain.[28] Thus, **10** and **11** were subjected to $^1O_2$ sensitized by 5,10,15,20-tetrakis(pentafluorophenyl)porphyrin and analysed for photodegradation products via liquid chromatography mass spectrometry (LCMS, Figure S12). We found that **11** degraded quickly (less than 1 hour) and cleaved at C-1' of the polymethine chain as anticipated.[28] Surprisingly, **10** reacted very little within one hour and did not display complete degradation by LCMS analysis until 17 hours. Unlike its oxygen counterpart, **10** degraded into a multitude of products suggesting that silicon incorporation deactivated the $^1O_2$ reactivity to the C-1' position of the polymethine chain.

We also compared the chemical stability of oxygen (**8**, **11**) and silicon polymethines (**7**, **10**) in dimethyl sulfoxide (Figure S13-16). All fluorophores appeared to favour the heterocycle peak in acidic conditions. However, the oxygen congeners (**8**, **11**) showed higher stability in basic conditions over a 24 h time period than the silicon polymethines (**7**, **10**), where there was complete loss of signal.

In summary, we have demonstrated that incorporation of silicon into polymethine dyes is a valid approach to red shift this class of fluorophores and is on par with vinylene chain extension. We prepared tri- and pentamethines with xanthene-derived hetereocycles which were 70–100 nm red-shifted compared to oxygen analogues, resulting in emission at 913 nm and 1006 nm, respectively. Our computations demonstrate that the higher lying LUMO energies of the oxygen analogues result from destabilizing lone pair interactions absent in their novel silicon counterparts. The silicon-containing polymethines had advantageous photostability, six to ten-fold more than their oxygen counterparts. The xanthene-derived heterocycles, while providing an efficient avenue for the synthesis of the first silicon polymethine dyes, also promoted ground state desymmetrization, which resulted in a broad, bimodal absorption spectrum and a decreased presence of the emissive species. The Wigner-sampled structures demonstrate that these accessible non-equilibrium structures contribute to the absorbance peak at 663 nm for **7** and **10**. Looking forward, the implementation of silicon into polymethine heterocycles that do not promote desymmetrization should provide avenues for the creation of deeply red-shifted (>900 nm) fluorophores with high

photostability. Strategies for developing dyes within these regions of the electromagnetic spectrum are of significant interest to the materials and biomedical communities.

Supplementary Material

Refer to Web version on PubMed Central for supplementary material.

Acknowledgements

references

1. Lavis LD and Raines RT, ACS Chem. Biol, 2008, 3, 142–155. [PubMed: 18355003]

2. Frangioni JV, Curr. Opin. Chem. Biol, 2003, 7, 626–634. [PubMed: 14580568]

3. Weissleder R, Nat. Biotechnol, 2001, 19, 316–317. [PubMed: 11283581]

4. Fu M, Xiao Y, Qian X, Zhao D and Xu Y, Chem. Commun, 2008, 1780.

5. Yamaguchi S and Tamao K, J. Chem. Soc. Dalt. Trans, 1998, 3693–3702.

6. Grimm JB, Brown TA, Tkachuk AN and Lavis LD, ACS Cent. Sci, 2017, 3, 975–985. [PubMed: 28979939]

7. Lukinavi ius G, Umezawa K, Olivier N, Honigmann A, Yang G, Plass T, Mueller V, Reymond L, Corrêa IR Jr, Luo Z-G, Schultz C, Lemke EA, Heppenstall P, Eggeling C, Manley S and Johnsson K, Nat. Chem, 2013, 5, 132–139. [PubMed: 23344448]

8. Kushida Y, Nagano T and Hanaoka K, Analyst, 2015, 140, 685–695. [PubMed: 25380094]

9. Choi A and Miller SC, Org. Lett, 2018, 20, 4482–4485. [PubMed: 30014702]

10. Ikeno T, Nagano T and Hanaoka K, Chem. - An Asian J, 2017, 12, 1435–1446.

11. Li C, Wang T, Li N, Li M, Li Y, Sun Y, Tian Y, Zhu J, Wu Y, Zhang D and Cui X, Chem. Commun, 2019, 55, 11802.

12. Bricks JL, Kachkovskii AD, Slominskii YL, Gerasov AO and Popov SV, Dye. Pigment, 2015, 121, 238–255.

13. Shandura MP, Poronik YM and Kovtun YP, Dye. Pigment, 2005, 66, 171–177.

14. Detty MR and Murray BJ, J. Org. Chem, 1982, 47, 5235–5239.

15. Pastierik T, Šebej P, Medalová J, Štacko P and Klán P, J. Org. Chem, 2014, 79, 3374–3382. [PubMed: 24684518]

16. Tolbert LM and Zhao X, J. Am. Chem. Soc, 1997, 119, 3253–3258.

17. Tolbert LM, Acc. Chem. Res, 1992, 25, 561–568..

18. Vasyluk SV, Viniychuk OO, Poronik YM, Kovtun YP, Shandura MP, Yashchuk VM and Kachkovsky OD, J. Mol. Struct, 2011, 990, 6–13.

19. Hu H, V Przhonska O, Terenziani F, Painelli A, Fishman D, Ensley TR, Reichert M, Webster S, Bricks JL, Kachkovski AD, Hagan Ae DJ and Van Stryland EW, Phys. Chem. Chem. Phys, 2013, 15, 7666. [PubMed: 23591769]

20. Zhao Y and Truhlar DG, Theor. Chem. Acc, 2008, 120, 215–241.

21. Gaussian 16, Revision A.03, M. J. Frisch, G. W. Trucks, H. B. Schlegel, G. E. Scuseria, M. A. Robb, J. R. Cheeseman, G. Scalmani, V. Barone, G. A. Petersson, H. Nakatsuji, X. Li, M. Caricato, A. V. Marenich, J. Bloino, B. G. Janesko, R. Gomperts, B. Mennu, 2016.

22. Head-Gordon M, Rico RJ, Oumi M and Lee TJ, Chem. Phys. Lett, 1994, 219, 21–29.

23. Head-Gordon M, Maurice D and Oumi M, Chem. Phys. Lett, 1995, 246, 114–121.

24. Neese F, WIREs Comput. Mol. Sci, 2018, 8, 1327.

25. Neese F, WIREs Comput. Mol. Sci, 2012, 2, 73–78.

26. Thimsen E, Sadtler B and Berezin MY, Nanophotonics, 2017, 6, 1043–1054.

27. Terenziani F, V Przhonska O, Webster S, Padilha LA, Slominsky YL, Davydenko IG, Gerasov AO, Kovtun YP, Shandura MP, Kachkovski AD, Hagan DJ, Van Stryland EW and Painelli A, J. Phys. Chem. Lett, 2010, 1, 1800–1804.

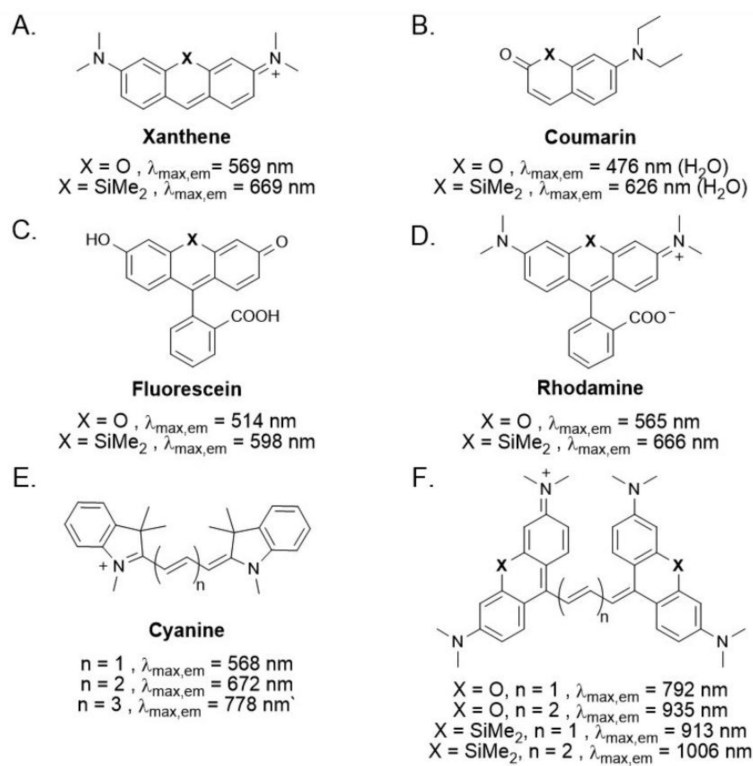28. Nani R, Kelley JA, Ivanic J and Schnermann MJ, Chem. Sci, 2015, 6, 6556–6563. [PubMed: 26508998]
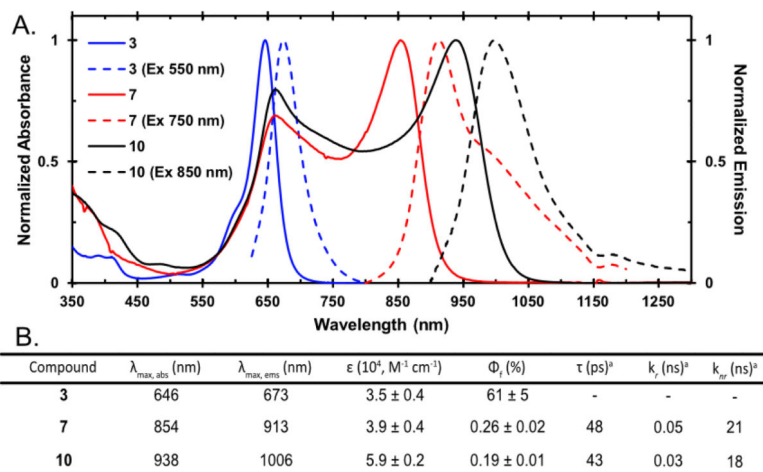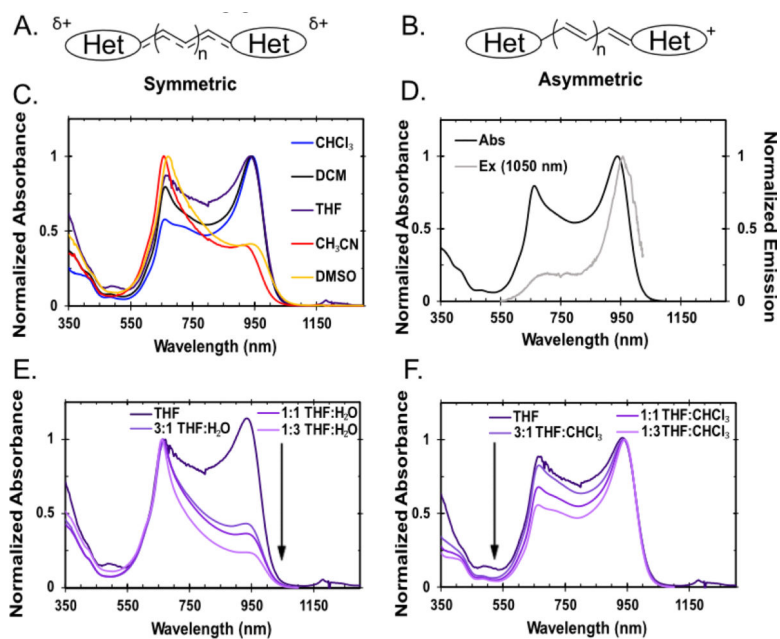
Figure 1.
Fluorophore scaffolds. A) Xanthene scaffold, the first fluorophore where silicon was incorporated.[4] B) Coumarin scaffold.[11] C) Fluorescein scaffold.[10] D) Rhodamine scaffold.[10] E) Cyanine scaffold: a classic polymethine dye.[12] F) This work on silicon polymethines and their oxygen counterparts.[13]
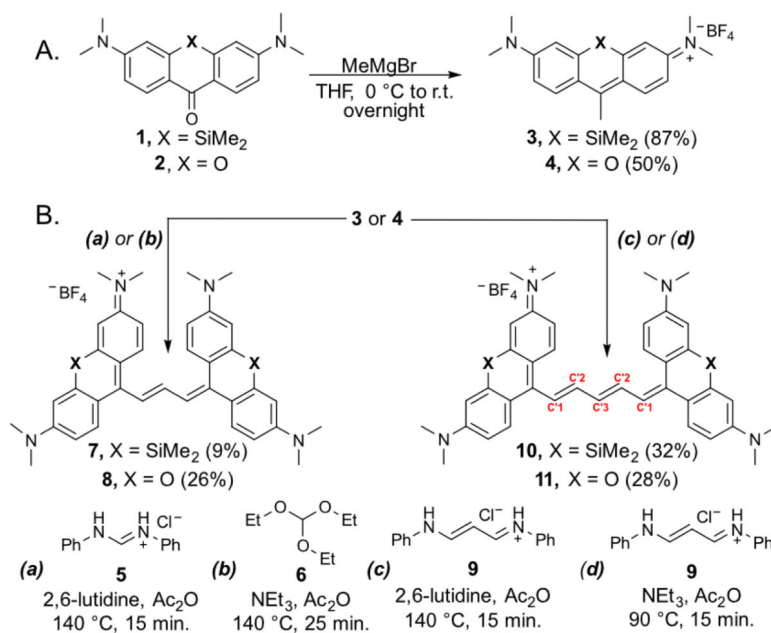
Scheme 1.
Synthesis of silicon and oxygen fluorophores studied herein. A) Heterocycle synthesis. B) Polymethine dye synthesis. For **7**, conditions **(a)**. For **8**, conditions **(b)**. For 10, conditions **(c)**. For **11**, conditions **(d)**.
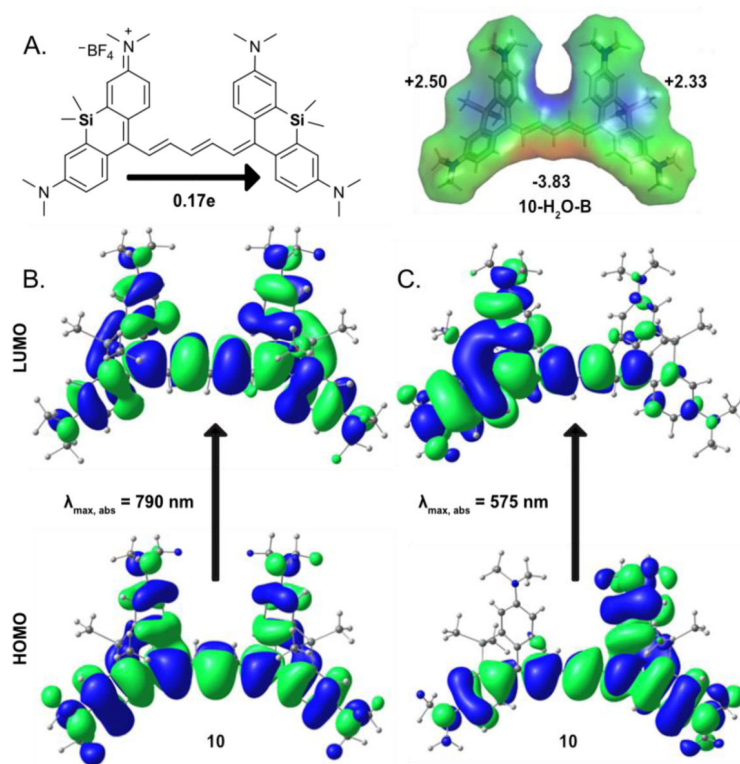
Figure 2.
Photophysical data of silicon fluorophores. A) Normalized absorbance (solid) and emission (dotted) in dichloromethane (DCM). B) Photophysical characterization of **3, 7, 10** in DCM. [a]Error and experimental in detail in Figure S8.
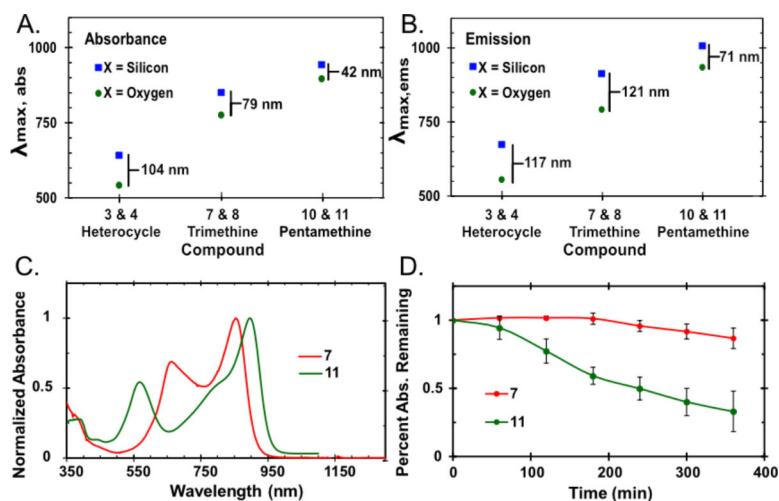
Figure 3.
A/B) Schematic of symmetric state (delocalized charge, A) and asymmetric state (dipolar, charge is localized on one heterocycle, B). C) Absorbance of **10** (normalized to λ_{max}) in a range of nonpolar and polar solvents. D) Normalized absorption spectra (Abs, black) and excitation spectra (Ex, grey, excitation from 515–1025 nm and collection 1050 nm) of **10** in DCM. E) Absorption spectra of **10** normalized at 663 nm in a solution of tetrahydrofuran (THF, 0.01 mM) supplemented with increasing amounts of H_2O. F) Absorption spectra of **10** normalized at 938 nm in a solution of THF (0.01 mM) supplemented with increasing amounts of $CHCl_3$.

Figure 4.
A) Conformer **10-H₂O-B** shows desymmetrization of 0.17e charge transfer toward the right heterocycle represented schematically and by electron density map. B) Frontier molecular orbitals of Wigner sampled structures of **10** computed with CIS(D)/cc-pvdz-RI correspond to $\lambda_{max,abs}$ of 790 nm, show complete electron delocalization. C) HOMO and LUMO of sampled structures of **10** with predicted $\lambda_{max,abs}$ of 575 nm show asymmetric character in their electronic structure.

Figure 5.

Comparison of silicon and oxygen xanthene polymethines. A/B) λ_{max} of silicon- (blue square) and oxygen- (green circle) containing polymethine fluorophores in DCM. The values depicted on the plot indicate the degree of red-shift imparted by silicon. A) Absorbance. B) Emission. C) Normalized absorbance spectra of **7** and **11** in DCM. D) Percent absorbance remaining at $\lambda_{max,abs}$ of **7** and **11** with continuous irradiation at 730 nm (146 mW/cm^2) over 6 hours. Error is the standard deviation of three experiments.